

Two-Dimensional NbS₂ Gas Sensors for Selective and Reversible NO₂ Detection at Room Temperature

Yeonhoo Kim,^{#,†,‡,§,||} Ki Chang Kwon,^{#,†,§,||} Sungwoo Kang,^{#,†} Changyeon Kim,[†] Tae Hoon Kim,[†] Seung-Pyo Hong,[†] Seo Yun Park,[†] Jun Min Suh,^{†,§} Min-Ju Choi,[†] Seungwu Han,^{*,†} and Ho Won Jang^{*,†,§}

[†]Department of Materials Science and Engineering, Research Institute of Advanced Materials, Seoul National University, Seoul 08826, Republic of Korea

[‡]Center for Integrated Nanotechnologies, Los Alamos National Laboratory, Los Alamos, New Mexico 87544, United States

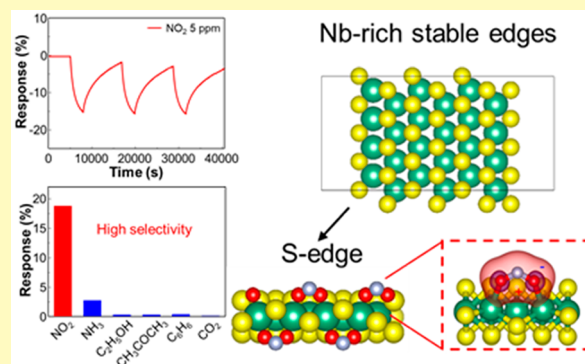
[§]School of Chemical Engineering and Materials Science, Integrative Research Center for Two-Dimensional Functional Materials, Institute of Interdisciplinary Convergence Research, Chung-Ang University, Seoul 06974, Republic of Korea

^{||}SZU-NUS Collaborative Innovation Center for Optoelectronic Science & Technology, College of Optoelectronic Engineering, Shenzhen University, Shenzhen 518060, China

Supporting Information

ABSTRACT: Transition metal dichalcogenides (TMDs) have attracted enormous attention in diverse research fields. Especially, gas sensors are considered in a promising application exploiting TMDs. However, the studies are confined to only major TMDs such as MoS₂ and WS₂. Particularly, the chemoresistive sensing properties of two-dimensional (2D) NbS₂ have never been explored. For the first time, we report room temperature NO₂ sensing characteristics of 2D NbS₂ nanosheets and the sensing mechanisms using first-principles calculations based on density functional theory. The results demonstrate that the NbS₂ edges possessing different configurations depending on synthetic conditions differ in the sensing ability of the TMD nanosheets. This study not only broadens the potential of 2D NbS₂ for gas sensing applications, but also presents the important role of edge configuration of TMDs depending on synthetic conditions for further studies.

KEYWORDS: 2D materials, niobium disulfide, gas sensors, DFT calculations, NO₂ detection



Two-dimensional (2D) materials such as graphene-based materials, metal oxide nanosheets, and transition metal dichalcogenides (TMDs) have received the significant attention in diverse research fields.^{1–12} Particularly, 2D TMDs are considered as prospective materials for varied applications such as field-effect transistors, catalysts, heterostructures, composite materials, and sensors due to their unique electrical properties.^{9,13–17} Among the various research fields, sensors are the most adequate to deploy the superb properties of 2D TMDs as they possess advantages in high surface-to-volume ratio, numerous active edge sites, and tunable electrical properties. Therefore, further research on sensing characteristics of 2D TMDs is essential for achieving high performance sensing devices.^{17–29} Nevertheless, chemoresistive sensing properties of 2D NbS₂ have never been explored since studies on NbS₂ have been weighted toward other properties.^{30–35} Recently, the nature of 2D NbS₂ has given the impression of having great potential in gas sensing applications through other research fields such as catalysis, hydrogen evolution reactions, and synthetic studies, since the

studies have demonstrated that 2D NbS₂ possesses a huge number of active edge sites which play a key role in chemical detection.^{33,36,37}

NO₂ gas is one of the major gas species emitted from industrial fumes and internal combustion engines of automobiles resulting in air pollution and health problems. It is well-known that exposure to ppm levels of NO₂ gas can have adverse effects on the human body.^{38–40} Also, it contributes to the formation of photochemical smog, which can have significant impacts on human health. For these reasons, various types of gas sensors including electrochemical, optical, and chemoresistive sensors have been developed to monitor and control the concentration of NO₂ in ambient air. Especially, the chemoresistive type of gas sensor is a promising platform for future electronics due to their advantages in easy operating systems and simple device structures. The

Received: May 30, 2019

Accepted: July 24, 2019

Published: July 24, 2019

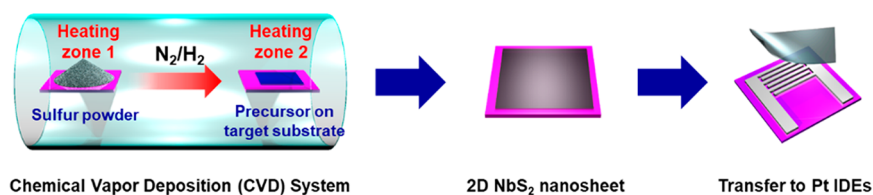


Figure 1. Fabrication procedure of 2D NbS₂ nanosheet gas sensors.

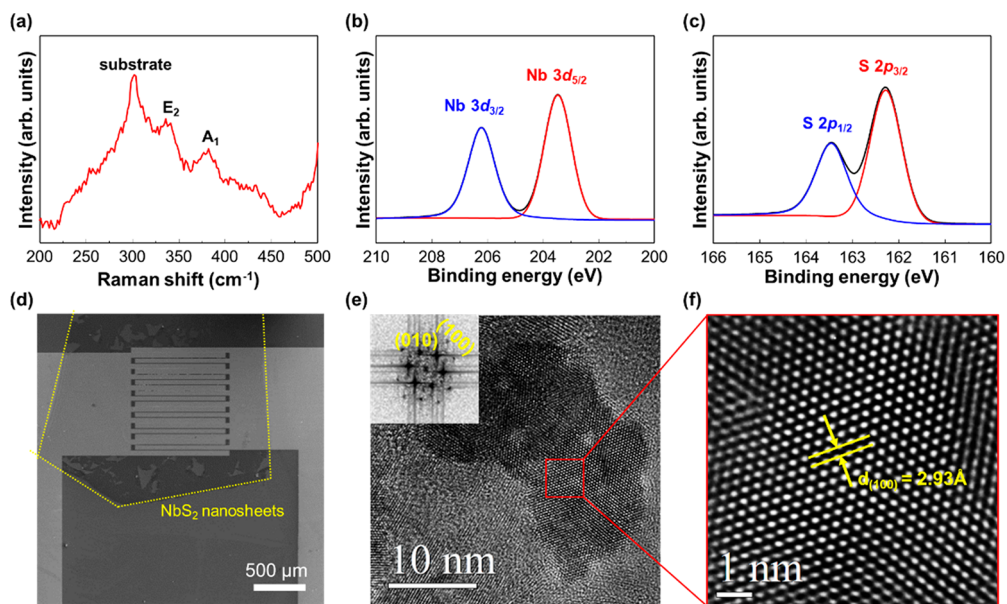


Figure 2. Basic material characterization of NbS₂ nanosheets. (a) Raman spectra of synthesized NbS₂ nanosheets. High-resolution XPS core level spectra of NbS₂ nanosheet for (b) Nb 3d and (c) S 2p. (d) Scanning electron microscopy (SEM) image of NbS₂ nanosheets on Pt-IDE substrate. (e,f) Transmission electron microscopic (TEM) images of NbS₂ nanosheet with different magnifications. Inset figure of (e) is FFT pattern of NbS₂ nanosheets.

advantages satisfy the requirements for next-generation electronics such as in the Internet of Things and wearable devices.

Here, for the first time, we report chemoresistive gas sensing characteristics of 2D NbS₂ nanosheets. The NbS₂ nanosheets were synthesized in thermal chemical vapor deposition (CVD) system through sulfurization of the Nb precursor which is coated on a target substrate. The synthesized nanosheets are transferred onto Pt interdigitated electrodes (IDEs). The device exhibited stable room temperature NO₂ gas sensing ability. The sensing mechanisms were investigated by first-principles calculations based on density functional theory. The theoretical calculation revealed that the composition and configuration of active edge sites play an important role in detection of NO₂ molecules. On the contrary, NO₂ molecules were not adsorbed on clean surfaces of 2D NbS₂. Since the sensing properties and investigation of sensing mechanisms of 2D NbS₂ nanosheets have never been accomplished yet, this work will be of great importance for future studies on sensing applications employing diverse 2D TMDs.

EXPERIMENTAL SECTION

Synthesis of NbS₂ Nanosheets. The precursor solution was prepared by dissolving niobium(V) chloride (NbCl₅, Sigma-Aldrich, 99.9% metals basis) in ethylene glycol (Sigma-Aldrich, 99.8% anhydrous) at a concentration of 100 mM. The precursor solution was spin-coated on cleaned SiO₂ (300 nm)/Si substrates at 3500 rpm for 60 s. The spin-coated substrate was preannealed on a hot plate at 50 °C to evaporate the residual solvents. The high purity hydrogen

(H₂) and nitrogen (N₂) gases were used for the sulfurization process in a thermal CVD system with dual furnaces. First, the temperature of the CVD furnace (Heater #2) for the precursor-coated sample was increased to 700 °C under the flow of H₂ and N₂ at 1 Torr during 30 min. The flow rate of H₂ and N₂ was set at 100 and 500 sccm, respectively, by using mass flow controllers. After 30 min, the CVD furnace (Heater #1) with temperature of 300 °C for S powder was moved through a sliding rail to the set position to evaporate the S powder for the sulfurization process. The sulfurization process was started slowly under a constant flow of H₂ and N₂ gas and maintained for 30 min. Finally, both furnaces were cooled down to room temperature with a rate of 20 °C/min.

Sensor Fabrication. Interdigitated electrodes (IDEs) were fabricated by depositing Pt/Ti (100/30 nm thick) on SiO₂/Si substrates (300 nm/500 μm thick) using an e-beam evaporator after patterning via photolithography. Twenty electrodes were placed in an area of 1 mm × 1 mm with a distance of 5 μm between them. The IDE-patterned substrates were cleaned by sonication in acetone and isopropanol, followed by drying in N₂ gas. The synthesized NbS₂ nanosheets were transferred onto the active area of Pt-IDE by the conventional wet transfer method.

Sensor Measurements. The gas sensing properties of the NbS₂ sensors were measured from room temperature to ~100 °C. As the flow gas was changed from dry air to a calibrated test gas (balanced with dry air, Sinjin Gases), the variation in the sensor resistance was monitored using a source measurement unit (Keithley 2365B). A constant flow rate of 1000 sccm was used for dry air and the test gas. The sensor resistance was measured at a DC bias voltage of 0.5 V. The response of the sensors ($\Delta R/R_0$) was accurately determined by measuring the baseline resistances of the sensors in dry air and the saturated resistances after exposure to the test gas. Gas flow was

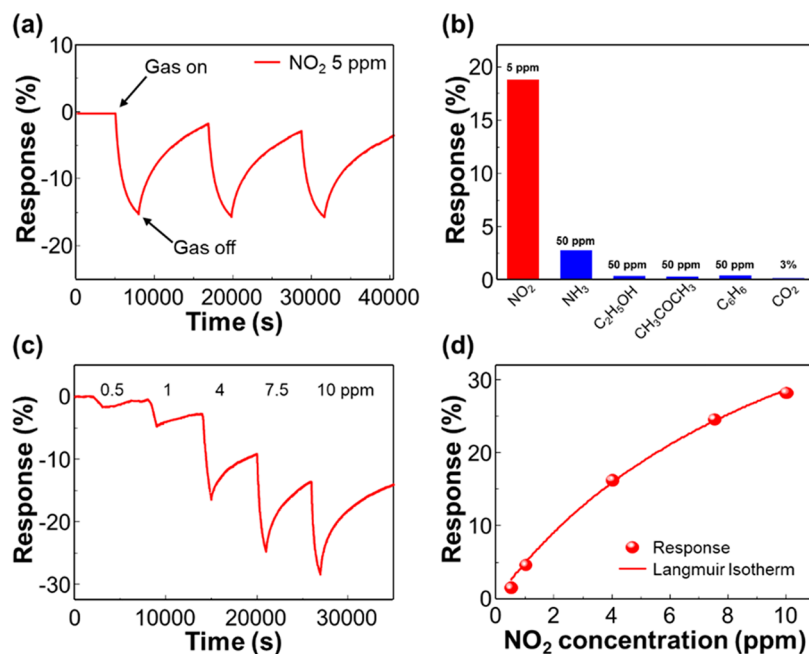


Figure 3. (a) Sensing curves of the NbS₂ gas sensor upon exposure to three consecutive pulses of 5 ppm of NO₂. (b) Sensing responses to 5 ppm of NO₂, 50 ppm of NH₃, C₂H₅OH, CH₃COCH₃, and C₆H₆, and 3% of CO₂. (c) Sensing curves of the NbS₂ gas sensor to the different concentration of NO₂. (d) Langmuir isotherm fit of the responses as a function of NO₂ concentration at room temperature.

controlled using mass flow controllers, and all the measurements were recorded using a computer over a GPIB interface.

Calculations. All density functional theory (DFT) calculations were performed using the Vienna ab initio simulation package (VASP).⁴¹ The electron–ion interaction is represented by projected-augmented wave (PAW) potential.⁴² We employ the Perdew–Burke–Ernzerhof (PBE) version of the gradient generalized approximation for the exchange–correlation functional.⁴³ A plane-wave cutoff is set to 500 eV. To illustrate the edge site of NbS₂, the six-layer thickness of infinite stripe structure is used. The Brillouin zone is sampled by 12 × 12 × 1 Monkhorst–Pack mesh for the unit cell and 3 × 1 × 1 Monkhorst–Pack mesh for the striped structures. All the atomic coordinates were relaxed within 0.03 eV Å⁻¹. The simulation cell for NO₂ adsorption is obtained by multiplying the periodicity by 6-fold to calculate the adsorption free energies (G_{ad}).

RESULTS AND DISCUSSION

2D NbS₂ nanosheets are synthesized by a facile fabrication process (Figure 1). A two-furnace chemical vapor deposition (CVD) system was employed. The temperature of the sulfur powder was elevated to 300 °C in the first heating zone, and NbS₂ precursor was spin-coated onto SiO₂/Si substrates. The substrates with NbS₂ precursor were heated at 700 °C with flowing N₂ (500 sccm) and H₂ (100 sccm) gas in the second heating zone.^{31,42,43} The synthesized 2D NbS₂ nanosheets were obtained as attached on the substrate and transferred onto Pt interdigitated electrodes (IDEs) of 5 μm interspacing. For the transfer process, the as-synthesized sample was coated with PMMA. The PMMA/NbS₂ nanosheets were separated from the SiO₂/Si substrates by immersion in a bath of HF and buffered oxide etchant, and the separated films were transferred onto the Pt-IDEs. Finally, the PMMA supporting polymer layer on the NbS₂ nanosheets was removed by a simple acetone treatment. After that, the final device was measured in a tube furnace for gas sensing properties at room temperature.

To investigate the atomic vibration mode of synthesized NbS₂ nanosheet, the Raman spectroscopy was performed as

shown in Figure 2a. There are four different Raman active modes which are A modes (A₁ and A₂, out-of-plane atomic vibration) and E modes (E₁ and E₂, in-plane atomic vibration).³³ In Figure 2a, there are two distinguishable peaks at near 330 and 386 cm⁻¹ for synthesized NbS₂ nanosheets. It is consistent with previous reports about the bulk and nanostructured 3R-type rhombohedral structure of NbS₂ crystals.⁴⁶

When the growth temperature increased to 900 °C, the NbCl₅ precursor was fully decomposed and transformed to the NbO₂ phase which is evaluated by the following evidence. In the Raman spectra (SI Figure S1), the two peaks corresponding to NbO₂ were observed after increasing growth temperature. Therefore, the thermolysis temperature is an important factor to get NbS₂ nanosheets instead of NbO₂ film.

The X-ray photoemission spectroscopy (XPS) is conducted to verify the atomic composition of synthesized 2D NbS₂ nanosheets as shown in Figure 2b and c. The XPS survey scans of 2D NbS₂ nanosheets are displayed in Figure S2. The peaks of Nb 3d_{3/2} and Nb 3d_{5/2} were located at 206.2 and 203.5 eV and the peaks of S 2p_{3/2} and S 2p_{1/2} are observed at 162.6 and 163.5 eV, respectively.^{44,45} The atomic ratio of Nb to S is ~2.08 which is in good agreement with the previous reports.^{33,46}

Furthermore, there are no chlorine peaks on synthesized NbS₂ nanosheets, which means the NbCl₅ solution precursor was fully decomposed during the high-temperature CVD process. Scanning electron microscopy (SEM) and energy dispersive spectroscopy (EDS) were carried out to confirm the surface morphology and atomic ratio of transferred NbS₂ nanosheets on Pt-IDE substrate (SI Figure S2). The NbS₂ nanosheets were transferred onto the active area of the gas sensing device after the conventional wet transfer method, as displayed in Figure 2d. The transferred NbS₂ film on the SiO₂ substrate was characterized by optical and atomic force microscopy (AFM) (SI Figure S3). The film was continuous

Table 1. Comparison of NO₂ Sensing Performances Demonstrated in This Work with Previous Reports in the Literature

Sensing materials	Sensing Temp. (°C)	NO ₂ conc. (ppm)	Ambient	Response (%)	Recovery (%)	Detection limit	ref.
NbS ₂	27	5	Air	~18%	~90%	241.02 ppb	This Work
WS ₂	27	100	Air	~9%	~10%	-	24
Structured	27	100	N ₂	~10%	~20%	-	54
MoS ₂ /MoS ₂	27	100	N ₂	~50%	~0%	-	23
MoS ₂ /SnO ₂	27	5	Air	~5%	~90%	500 ppb	49
hybrid MoS ₂	27	1.2	N ₂	~7%	~10%	-	27
MoS ₂ /graphene hybrid	200	3	N ₂	~15%	~95%	100 ppb	55
Graphene	27	1	N ₂	~4%	~0%	-	56
rGO	27	5	N ₂	~12%	~15%	-	57

and the thickness of NbS₂ nanosheets was measured to be 5 nm. In addition, the EDS spectra clearly show that the atomic ratio of Nb to S is around 2.06, which is consistent with the XPS results in Figure 2b and c. In order to verify the atomic structure of the synthesized NbS₂ nanosheet, transmission electron microscopy (TEM) was conducted, as shown in Figure 2e and f. The single set of diffraction spots can be indexed by a hexagonal lattice along the *c*-axis, and the lattice constant can be estimated by the *d*-spacing measured from the diffraction patterns as displayed in the inset figure of the fast Fourier transform (FFT) pattern. The lattice plane distance of 0.293 nm is well-matched with the (010) and (100) lattice distance. According to the atomic structure of 3R-type NbS₂, each Nb atom is sixfold coordinated, hexagonally packed between two, threefold coordinated S atoms, and the S–Nb–S layers are weakly bound to other layers by weak van der Waals force. Our TEM results show good agreement with Raman spectra results and previous results as well.^{33,46}

Figure 3a exhibits dynamic sensing transients of the NbS₂ gas sensor upon exposure to three consecutive pulses of NO₂ gas at room temperature. Response and recovery times were 3000 and 9000 s, respectively. The real-time resistance curves were presented in Figure S4a. Although the recovery time was very long, it presents the reversible sensing properties of 2D NbS₂ nanosheets, and the reaction times can be improved by further studies such as modification of surface chemistry of 2D materials.^{7,8,19,20,26,47–49} The sensing curve is gradually saturated. Since the time scale in Figure 3 is too large to identify the saturation, a sensing curve is separately added in Figure S4b. To check the long-term stability and the influence of humidity, the sensor was measured after 15 and 90 days from the first measurement and in a range of relative humidity (SI Figure S5). Responses of the sensor were measured to be 14.7 and 11.7 after 15 and 90 days, respectively. In relative humidity from 10% to 50%, the sensor exhibits reversible sensing behavior. The gas selectivity of the sensor was displayed in Figure 3b. The sensing responses upon exposure to NO₂, NH₃, C₂H₅OH, CH₃COCH₃, C₆H₆, and CO₂ were measured to be 18.8%, 2.79%, 0.35%, 0.32%, 0.44%, and 0.18%, respectively. Each sensing curve for different gases can be found in Figure S6. The NbS₂ sensor exhibited much higher selectivity upon exposure to NO₂ in comparison with the responses to other gases. In order to investigate the sensing properties of the NbS₂ nanosheet to NO₂ gas, the NbS₂ sensor was exposed to different NO₂ concentrations ranging from 0.5 to 10 ppm, as displayed in Figure 3c. The responses of the NbS₂ sensor to 0.5, 1, 4, 7.5, and 10 ppm of NO₂ are 1.53, 4.66, 16.3, 24.7, and 28.32, respectively, as shown in Figure 3d. The correlation between gas response and gas concentration was in good agreement with the Langmuir adsorption isotherm

model.^{50,51} Linear regression fit was also employed to confirm the linear relationship between the responses and the NO₂ concentrations and calculate the theoretical detection limit (SI Figure S7). The gas responses as a function of NO₂ concentration showed high linearity with linear regression, *r*², 0.956. The theoretical detection limit was calculated to be 241.02 ppb.^{52,53}

The sensing properties including recovery rate, responsibility, and some other factors related to gas sensing are summarized in Table 1 to directly compare the sensing properties of 2D NbS₂ with other 2D materials such as MoS₂, WS₂, etc.^{54–57} Among the diverse 2D materials, sensing performances of pristine WS₂, MoS₂, graphene, and their hybrid composites which have been regarded as the most promising 2D materials for gas sensing in recent studies are presented. In Table 1, the response of 2D NbS₂ to NO₂ is much higher than that of the other sensors compared at the same gas concentration. The response of 2D NbS₂ is measured to be ~18% upon exposure to 5 ppm of NO₂. For 2D WS₂, however, the response is only ~9% when the device is exposed to a high concentration of NO₂, 100 ppm. Similar to the WS₂, MoS₂- and graphene-based sensors also exhibit lower sensing responses than that of the 2D NbS₂ sensors. Even though researchers synthesized structured TMDs and hybrid composites with TMDs to increase gas sensing responses, NO₂ responses were much lower than that of pristine 2D NbS₂ at the same gas concentration.^{43,49,50} In view of the recovery at room temperature, 2D NbS₂ sensor presents a reversible sensing behavior while the other 2D materials do not recover to initial states at room temperature. One of the major problems in gas sensing applications is gas selectivity. The other 2D materials have shown high response to more than two gas species including NO₂, NH₃, and volatile organic compounds (VOCs). On the contrary, the 2D NbS₂ gas sensors exhibit much higher selectivity to NO₂ gas. In addition to this, the theoretical detection limit of NbS₂ is very low, as low as 241.02 ppb. In view of the responses, 2D materials exhibit lower responses than those of gas sensors based on metal oxide semiconductors. However, metal oxides are brittle and nontransparent so that 2D materials are considered a leading candidate for next-generation electronics such as flexible, transparent, and wearable devices.⁵⁸

To explain the experimental results, we calculated the adsorption free energy (*G*_{ad}) using first-principles calculations based on the density functional theory. First, we calculated the adsorption free energy (*G*_{ad}) of the NO₂ molecule on a clean surface at temperature *T* and partial pressure *P* as follows:

$$G_{\text{ad}}(T, P) = G(\text{NbS}_2 + \text{NO}_2) - G(\text{NbS}_2) - \mu_{\text{NO}_2}(T, P) \quad (1)$$

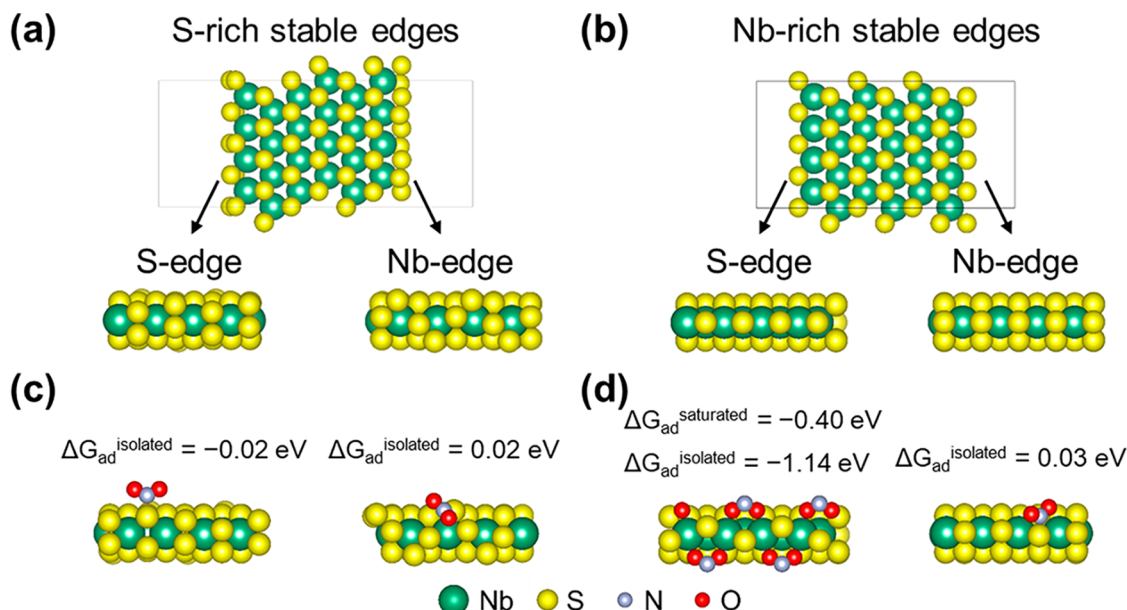


Figure 4. Stable edges of 2D NbS₂ synthesized under (a) S-rich and (b) Nb-rich conditions. The bottom schematic shows the configurations of stable S- and Nb-edges. Stable adsorption sites of NO₂ on (c) S- (left) and Nb-edges (right) of S-rich stable edges and (d) S- (left) and Nb-edges (right) of Nb-rich stable edges. The adsorption energies are displayed on the upper side of each schematic.

where $G(\text{NbS}_2 + \text{NO}_2)$ and $G(\text{NbS}_2)$ indicate the free energies of the NbS₂ surface with and without an NO₂ molecule adsorbed on clean NbS₂, respectively, and $\mu_{\text{NO}_2}(T, P)$ is the gas-phase chemical potential of the NO₂ molecule. The experimental conditions are considered in $\mu_{\text{NO}_2}(T, P)$ as follows:

$$\mu_{\text{NO}_2}(T, P) = \mu_{\text{NO}_2}(T, P^0) + k_b T \ln\left(\frac{P}{P^0}\right) \quad (2)$$

where P^0 is 1 atm. In addition,

$$\mu_{\text{NO}_2}(T, P^0) = \Delta H - T\Delta S \mu_{\text{NO}_2}(T, P^0) + \mu_{\text{NO}_2}(0\text{K}, P^0) \quad (3)$$

where ΔH and ΔS correspond to the enthalpy and entropy changes per molecule between T and 0 K at the standard pressure, respectively, which are obtained from thermodynamical tables.⁵⁹ In eq 3, $\mu_{\text{NO}_2}(0 \text{ K}, P^0)$ is equal to the total energy of the NO₂ molecule.

We calculated the G_{ad} of the NO₂ molecule on a clean surface and edge site of NbS₂. For the clean surface, G_{ad} is 0.25 eV, meaning that the NO₂ molecule would barely bind to the clean surface (SI Figure S8). For edge sites, we considered stable edge configurations of Nb- and S-edges depending on synthetic conditions (Nb-rich and S-rich conditions, respectively). G_{ad} (300 K, 10 ppm of NO₂) for each edge is shown in Figure 4. $G_{\text{ad}}^{\text{isolated}}$ and $G_{\text{ad}}^{\text{saturated}}$ denote the binding energies of NO₂ when the coverage of NO₂ molecules at the edge site is 0% (isolated) and 100% (saturated), respectively. $G_{\text{ad}}^{\text{isolated}}$ is calculated by eq 1 and $G_{\text{ad}}^{\text{saturated}}$ is defined as follows:

$$\begin{aligned} G_{\text{ad}}(T, P) &= G(\text{NbS}_2 + x_{\text{max}} \text{NO}_2) \\ &- G(\text{NbS}_2 + (x_{\text{max}} - 1) \text{NO}_2) \\ &- \mu_{\text{NO}_2}(T, P) \end{aligned} \quad (4)$$

where x_{max} is the maximum number of molecules at the edge site ($x_{\text{max}} = 4$ in this size of super cell). Among four edges in

Figure 4, only $G_{\text{ad}}^{\text{isolated}}$ of the S-edge at Nb-rich condition is negative enough (-1.14 eV) to adsorb NO₂ at 300 K. In addition, $G_{\text{ad}}^{\text{saturated}}$ of the S-edge at Nb-rich condition is -0.40 eV , which indicates that the S-edge is expected to adsorb NO₂ as much as possible. This is in agreement with the high sensitivity to NO₂ and steady increase in NO₂ response as shown in Figure 3.

In order to understand the charge transfer between NO₂ and NbS₂, we investigate the variation in the electron charge density of the S-edge of NbS₂ in Nb-rich condition upon adsorption of NO₂ (Figure 5). The blue and red charge

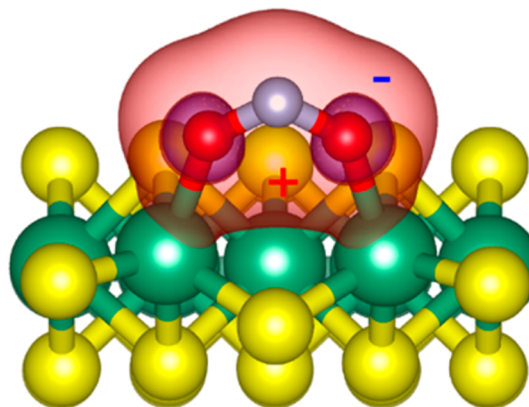


Figure 5. Bader charge analysis of adsorption of NO₂ on S-edge synthesized in Nb-rich condition.

distribution in Figure 5 indicate positive and negative change of electron densities, respectively, after adsorption of NO₂. The adsorption of NO₂ increases the charge density on the oxygen atoms on NO₂, while it decreases the charge density on the nitrogen atom. The Bader charge analysis shows that the charge density on the oxygen molecules increased by 0.27 e, whereas the charge density on the niobium molecules

decreased by -0.13 e. This confirms that the NO_2 molecule adsorbs on Nb molecules on the edge sites.

To analyze the sensing performance of NbS_2 in Figure 3, densities of states (DOS) of the S-edge site were compared before and after the NO_2 adsorption (Figure 6a and b,

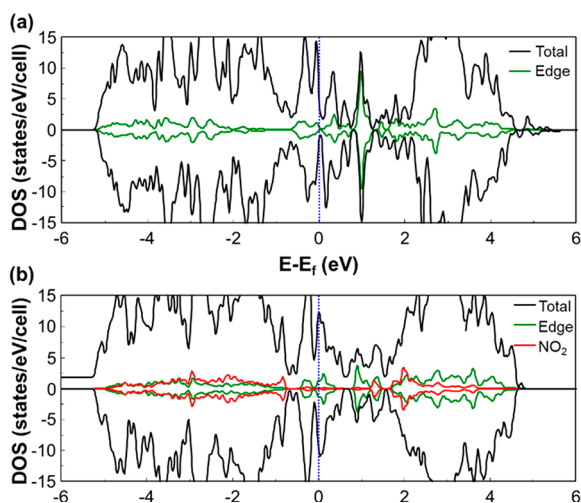


Figure 6. Density of states of entire NbS_2 and edge sites (a) before NO_2 adsorption and (b) after NO_2 adsorption.

respectively). After the adsorption, the projected DOS (PDOS) of NO_2 is delocalized over a large energy range (see the red line in Figure 6b). This signifies that the NO_2 molecular orbital and edge states are hybridized and subsequently have a strong bonding, which is consistent with low adsorption energy of NO_2 at the S-edge (Figure 4d). The change of atomic coordinates (Figure 4) and spatial charge distribution (Figure 5) of Nb and S atoms at the S-edge after adsorption of NO_2 also modulates the PDOS of NbS_2 (see the green line in Figure 6b). The PDOS of the edge site near the Fermi level is increased when NO_2 is adsorbed (SI Figure S9). This indicates that the carrier density of the edge site is increased when the NO_2 molecule is adsorbed, which accounts for the origin of the response of NO_2 sensor in Figure 3.

While the present study focuses on the interaction between NO_2 and NbS_2 , the oxygen in the atmosphere can also affect the sensing activity. $G_{\text{ad}}^{\text{isolated}}$ and $G_{\text{ad}}^{\text{saturated}}$ of the oxygen molecule at the S-edge in Nb-rich conditions are -1.57 eV and -0.41 eV, respectively (SI Figure S10a and b). These values are negative and comparable to NO_2 , which indicates that both NO_2 and O_2 bind to the edge site competitively. To verify the effect of NO_2 and O_2 on the sensing mechanism, we compare the density of states of the S-edge between various coverages of adsorbed O_2 and NO_2 (SI Figure S10c and d). Figure S10e shows that the density of states around the Fermi level increases with increasing proportion of NO_2 , which shows similar trends without the oxygen molecule in Figure S9.

Figure 7 shows the comparison of sensing properties in different temperatures ranging from room temperature to 100 °C. Despite the remarkable sensing properties at room temperature, we demonstrate that the sensing ability of NbS_2 can be tuned by temperature changes. According to the purposes and requirements of practical sensing applications, the tunable sensing abilities are important. The response and recovery t_{90} became much faster under 100 °C. This demonstrates that the NbS_2 nanosheets have a great potential

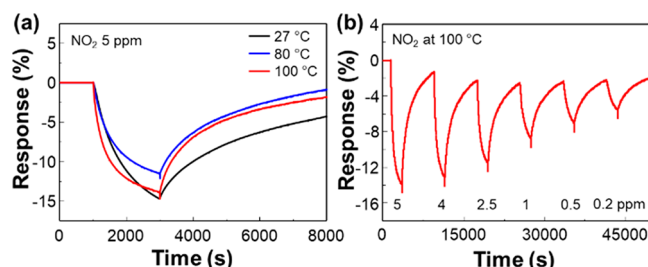


Figure 7. (a) Sensing curves of the 2D NbS_2 gas sensor at room temperature, 80 and 100 °C. (b) Response curves to different NO_2 concentrations from 200 ppb to 5 ppm.

in various applications with different purposes because the conventional metal oxide-based chemoresistive sensors only operate at certain temperatures, >150 °C, resulting in high power consumption and thermal safety issues. Furthermore, the 2D NbS_2 sensor exhibits the extremely high sensitivity at 100 °C showing response to under 200 ppb of NO_2 .

CONCLUSIONS

We have demonstrated synthesis of 2D NbS_2 nanosheets through thermolysis of the NbCl_5 solution precursor using chemical vapor deposition. Various material characterizations were conducted to verify the physical and chemical properties of synthesized NbS_2 nanosheets. The NbS_2 sensors exhibited reversible and selective NO_2 sensing performance at room temperature. Moreover, the sensing mechanisms are revealed by DFT calculations. The calculation revealed that the sensing properties of 2D NbS_2 can be modified by different edge configurations depending on synthetic conditions. The results demonstrated that 2D NbS_2 prepared by a facile synthesis process have great potential for future chemoresistive sensing applications.

ASSOCIATED CONTENT

Supporting Information

The Supporting Information is available free of charge on the ACS Publications website at DOI: [10.1021/acssensors.9b00992](https://doi.org/10.1021/acssensors.9b00992).

Raman spectra of NbS_2 and NbO_2 samples from different growth temperatures, XPS survey scan and AFM characterization of 2D NbS_2 nanosheets, response curves upon exposure to 5 ppm of NO_2 , response curves of 2D NbS_2 nanosheets to various gases at room temperature, linear fit of the responses as a function of NO_2 concentration at room temperature, adsorption energy of the NO_2 molecule on a clean surface at 300 K and 10 ppm of NO_2 , density of states of NO_2 adsorbed S-edge and bare S-edge in Nb-rich condition (PDF)

AUTHOR INFORMATION

Corresponding Authors

*E-mail: hwjang@snu.ac.kr. Phone: (+82)2-880-1720.

*E-mail: hansw@snu.ac.kr. Phone: (+82)2-880-1541.

ORCID

Yeonhoo Kim: [0000-0003-3057-3208](https://orcid.org/0000-0003-3057-3208)

Ki Chang Kwon: [0000-0002-4004-5372](https://orcid.org/0000-0002-4004-5372)

Jun Min Suh: [0000-0001-8506-0739](https://orcid.org/0000-0001-8506-0739)

Ho Won Jang: [0000-0002-6952-7359](https://orcid.org/0000-0002-6952-7359)

Author Contributions

#H. W. J. and S. H. conceived and supervised the project. Y. K. and T. K. measured the device and analyzed the results. K. C. K. and C. K. synthesized and characterized the NbS₂. S. K. and S. H. conducted the DFT calculations. S.-P. H. conducted TEM analysis. S. Y. P. and T. K. helped with experiments and data analysis. J. M. S. took the SEM images. M. C. carried out the XRD characterization. The manuscript was mainly written by H. W. J., and Y. K. All authors discussed the results and commented on the manuscript at all stages. Y. K., K. C. K., and S. K. contributed equally.

Notes

The authors declare no competing financial interest.

ACKNOWLEDGMENTS

This work was supported by LG Display under LGD-Seoul National University Incubation Program and the Institute of Engineering Research at Seoul National University, and performed, in part, at the Center for Integrated Nanotechnologies, an Office of Science User Facility operated for the U.S. Department of Energy (DOE) Office of Science. Los Alamos National Laboratory, an affirmative action equal opportunity employer, is managed by Triad National Security, LLC for the U.S. Department of Energy's NNSA, under contract 89233218CNA000001.

REFERENCES

- (1) Torrisi, F.; Coleman, J. N. Electrifying inks with 2D materials. *Nat. Nanotechnol.* **2014**, *9* (10), 738–739.
- (2) Sun, Z.; Martinez, A.; Wang, F. Optical modulators with 2D layered materials. *Nat. Photonics* **2016**, *10* (4), 227–238.
- (3) Sun, Z.; Liao, T.; Dou, Y.; Hwang, S. M.; Park, M.-S.; Jiang, L.; Kim, J. H.; Dou, S. X. Generalized self-assembly of scalable two-dimensional transition metal oxide nanosheets. *Nat. Commun.* **2014**, *5*, 3813.
- (4) Novoselov, K.; Mishchenko, A.; Carvalho, A.; Neto, A. C. 2D materials and van der Waals heterostructures. *Science* **2016**, *353* (6298), 461.
- (5) Mas-Balleste, R.; Gomez-Navarro, C.; Gomez-Herrero, J.; Zamora, F. 2D materials: to graphene and beyond. *Nanoscale* **2011**, *3* (1), 20–30.
- (6) Kim, Y. H.; Kim, S. J.; Kim, Y.-J.; Shim, Y.-S.; Kim, S. Y.; Hong, B. H.; Jang, H. W. Self-activated transparent all-graphene gas sensor with endurance to humidity and mechanical bending. *ACS Nano* **2015**, *9* (10), 10453–10460.
- (7) Kim, Y.; Choi, Y. S.; Park, S. Y.; Kim, T.; Hong, S.-P.; Lee, T. H.; Moon, C. W.; Lee, J.-H.; Lee, D.; Hong, B. H.; Jang, H. W. Au decoration of a graphene microchannel for self-activated chemoresistive flexible gas sensors with substantially enhanced response to hydrogen. *Nanoscale* **2019**, *11*, 2966–2973.
- (8) Kim, Y. H.; Park, J. S.; Choi, Y.-R.; Park, S. Y.; Lee, S. Y.; Sohn, W.; Shim, Y.-S.; Lee, J.-H.; Park, C. R.; Choi, Y. S.; Hong, B. H.; Lee, J. H.; Lee, W. H.; Lee, D.; Jang, H. W. Chemically fluorinated graphene oxide for room temperature ammonia detection at ppb levels. *J. Mater. Chem. A* **2017**, *5*, 19116–19125.
- (9) Fiori, G.; Bonaccorso, F.; Iannaccone, G.; Palacios, T.; Neumaier, D.; Seabaugh, A.; Banerjee, S. K.; Colombo, L. Electronics based on two-dimensional materials. *Nat. Nanotechnol.* **2014**, *9* (10), 768–779.
- (10) Chen, Z.; Wang, J.; Pan, D.; Wang, Y.; Noetzel, R.; Li, H.; Xie, P.; Pei, W.; Umar, A.; Jiang, L.; Li, N.; de Rooji, N. F.; Zhou, G. Mimicking a Dog's Nose: Scrolling Graphene Nanosheets. *ACS Nano* **2018**, *12* (3), 2521–2530.
- (11) Xu, T.; Liu, Y.; Pei, Y.; Chen, Y.; Jiang, Z.; Shi, Z.; Xu, J.; Wu, D.; Tian, Y.; Li, X. The Ultra-High NO₂ Response of Ultra-Thin

WS₂ Nanosheets Synthesized by Hydrothermal and Calcination Processes. *Sens. Actuators, B* **2018**, *259*, 789–796.

- (12) Wu, E.; Xie, Y.; Yuan, B.; Zhang, H.; Hu, X.; Liu, J.; Zhang, D. Ultrasensitive and Fully Reversible NO₂ Gas Sensing Based on pType MoTe₂ under Ultraviolet Illumination. *ACS Sens* **2018**, *3* (9), 1719–1726.

- (13) Yang, L.; Majumdar, K.; Liu, H.; Du, Y.; Wu, H.; Hatzistergos, M.; Hung, P.; Tieckelmann, R.; Tsai, W.; Hobbs, C. Chloride molecular doping technique on 2D materials: WS₂ and MoS₂. *Nano Lett.* **2014**, *14* (11), 6275–6280.

- (14) Voiry, D.; Yang, J.; Chhowalla, M. Recent strategies for improving the catalytic activity of 2D TMD nanosheets toward the hydrogen evolution reaction. *Adv. Mater.* **2016**, *28* (29), 6197–6206.

- (15) Podzorov, V.; Gershenson, M.; Kloc, C.; Zeis, R.; Bucher, E. High-mobility field-effect transistors based on transition metal dichalcogenides. *Appl. Phys. Lett.* **2004**, *84* (17), 3301–3303.

- (16) Liu, Y.; Weiss, N. O.; Duan, X.; Cheng, H.-C.; Huang, Y.; Duan, X. Van der Waals heterostructures and devices. *Nat. Rev. Mater.* **2016**, *1* (9), 16042.

- (17) Kim, Y. H.; Kim, K. Y.; Choi, Y. R.; Shim, Y.-S.; Jeon, J.-M.; Lee, J.-H.; Kim, S. Y.; Han, S.; Jang, H. W. Ultrasensitive reversible oxygen sensing by using liquid-exfoliated MoS₂ nanoparticles. *J. Mater. Chem. A* **2016**, *4* (16), 6070–6076.

- (18) Perrozzi, F.; Emamjomeh, S.; Paolucci, V.; Taglieri, G.; Ottaviano, L.; Cantalini, C. Thermal stability of WS₂ flakes and gas sensing properties of WS₂/WO₃ composite to H₂, NH₃ and NO₂. *Sens. Actuators, B* **2017**, *243*, 812–822.

- (19) Park, S. Y.; Lee, J. E.; Kim, Y. H.; Kim, J. J.; Shim, Y.-S.; Kim, S. Y.; Lee, M. H.; Jang, H. W. Room temperature humidity sensors based on rGO/MoS₂ hybrid composites synthesized by hydrothermal method. *Sens. Actuators, B* **2018**, *258*, 775–782.

- (20) Park, S. Y.; Kim, Y. H.; Lee, S. Y.; Sohn, W.; Lee, J. E.; Kim, D. H.; Shim, Y.-S.; Kwon, K. C.; Choi, K. S.; Yoo, H. J.; et al. Highly selective and sensitive chemoresistive humidity sensors based on rGO/MoS₂ van der Waals composites. *J. Mater. Chem. A* **2018**, *6* (12), 5016–5024.

- (21) O'Brien, M.; Lee, K.; Morrish, R.; Berner, N. C.; McEvoy, N.; Wolden, C. A.; Duesberg, G. S. Plasma assisted synthesis of WS₂ for gas sensing applications. *Chem. Phys. Lett.* **2014**, *615*, 6–10.

- (22) Lee, K.; Gatensby, R.; McEvoy, N.; Hallam, T.; Duesberg, G. S. High-performance sensors based on molybdenum disulfide thin films. *Adv. Mater.* **2013**, *25* (46), 6699–6702.

- (23) Late, D. J.; Huang, Y.-K.; Liu, B.; Acharya, J.; Shirodkar, S. N.; Luo, J.; Yan, A.; Charles, D.; Waghmare, U. V.; Dravid, V. P. Sensing behavior of atomically thin-layered MoS₂ transistors. *ACS Nano* **2013**, *7* (6), 4879–4891.

- (24) Ko, K. Y.; Song, J.-G.; Kim, Y.; Choi, T.; Shin, S.; Lee, C. W.; Lee, K.; Koo, J.; Lee, H.; Kim, J.; et al. Improvement of gas-sensing performance of large-area tungsten disulfide nanosheets by surface functionalization. *ACS Nano* **2016**, *10* (10), 9287–9296.

- (25) Kim, T. H.; Kim, Y. H.; Park, S. Y.; Kim, S. Y.; Jang, H. W. Two-dimensional transition metal disulfides for chemoresistive gas sensing: perspective and challenges. *Chemosensors* **2017**, *5* (2), 15.

- (26) Kim, J.-S.; Yoo, H.-W.; Choi, H. O.; Jung, H.-T. Tunable volatile organic compounds sensor by using thiolated ligand conjugation on MoS₂. *Nano Lett.* **2014**, *14* (10), 5941–5947.

- (27) He, Q.; Zeng, Z.; Yin, Z.; Li, H.; Wu, S.; Huang, X.; Zhang, H. Fabrication of flexible MoS₂ thin-film transistor arrays for practical gas-sensing applications. *Small* **2012**, *8* (19), 2994–2999.

- (28) Kwon, K. C.; Suh, J. M.; Lee, T. H.; Choi, K. S.; Hong, K.; Song, Y. G.; Shim, Y.-S.; Shokouhimehr, M.; Kang, C.-Y.; Kim, S. Y.; Jang, H. W. SnS₂ nanograins on porous SiO₂ nanorods template for highly sensitive NO₂ sensor at room temperature with excellent recovery. *ACS Sens* **2019**, *4*, 678–686.

- (29) Shim, Y.-S.; Kwon, K. C.; Suh, J. M.; Choi, K. S.; Song, Y. G.; Sohn, W.; Choi, S.; Hong, K.; Jeon, J.-M.; Hong, S.-P.; Kim, S.; Kim, S. Y.; Kang, C.-Y.; Jang, H. W. Synthesis of numerous edge sites in MoS₂ via SiO₂ nanorods platform for highly sensitive gas sensor. *ACS Appl. Mater. Interfaces* **2018**, *10*, 31594–31602.

- (30) Zhou, Y.; Wang, Z.; Yang, P.; Zu, X.; Yang, L.; Sun, X.; Gao, F. Tensile strain switched ferromagnetism in layered NbS₂ and NbSe₂. *ACS Nano* **2012**, *6* (11), 9727–9736.
- (31) Zhang, Y.; Yin, L.; Chu, J.; Shifa, T. A.; Xia, J.; Wang, F.; Wen, Y.; Zhan, X.; Wang, Z.; He, J. Edge-epitaxial growth of 2D NbS₂-WS₂ lateral metal-semiconductor heterostructures. *Adv. Mater.* **2018**, *30* (40), 1803665.
- (32) Guillamón, I.; Suderow, H.; Vieira, S.; Cario, L.; Diener, P.; Rodiere, P. Superconducting density of states and vortex cores of 2H-NbS₂. *Phys. Rev. Lett.* **2008**, *101* (16), 166407.
- (33) Ge, W.; Kawahara, K.; Tsuji, M.; Ago, H. Large-scale synthesis of NbS₂ nanosheets with controlled orientation on graphene by ambient pressure CVD. *Nanoscale* **2013**, *5* (13), 5773–5778.
- (34) Fu, Q.; Wang, X.; Zhou, J.; Xia, J.; Zeng, Q.; Lv, D.; Zhu, C.; Wang, X.; Shen, Y.; Li, X.; et al. One-Step Synthesis of Metal/Semiconductor Heterostructure NbS₂/MoS₂. *Chem. Mater.* **2018**, *30* (12), 4001–4007.
- (35) Bark, H.; Choi, Y.; Jung, J.; Kim, J. H.; Kwon, H.; Lee, J.; Lee, Z.; Cho, J. H.; Lee, C. Large-area niobium disulfide thin films as transparent electrodes for devices based on two-dimensional materials. *Nanoscale* **2018**, *10* (3), 1056–1062.
- (36) Noh, S. H.; Hwang, J.; Kang, J.; Seo, M. H.; Choi, D.; Han, B. Tuning the catalytic activity of heterogeneous two-dimensional transition metal dichalcogenides for hydrogen evolution. *J. Mater. Chem. A* **2018**, *6* (41), 20005–20014.
- (37) Gopalakrishnan, D.; Lee, A.; Thangavel, N. K.; Arava, L. M. R. Facile synthesis of electrocatalytically active NbS₂ nanoflakes for an enhanced hydrogen evolution reaction (HER). *Sustain. Energy Fuels* **2018**, *2* (1), 96–102.
- (38) Richters, A.; Kuraitis, K. Inhalation of NO₂ and blood borne cancer cell spread to the lungs. *Arch. Environ. Health* **1981**, *36* (1), 36–39.
- (39) Guidotti, T. L. The higher oxides of nitrogen: inhalation toxicology. *Environ. Res.* **1978**, *15* (3), 443–472.
- (40) Blomberg, A.; Krishna, M. T.; Bocchino, V.; Biscione, G. L.; Shute, J. K.; Kelly, F. J.; Frew, A. J.; Holgate, S. T.; Sandstrom, T. The inflammatory effects of 2 ppm NO₂ on the airways of healthy subjects. *Am. J. Respir. Crit. Care Med.* **1997**, *156* (2), 418–424.
- (41) Kresse, G.; Hafner, J. Ab initio molecular dynamics for liquid metals. *Phys. Rev. B: Condens. Matter Mater. Phys.* **1993**, *47* (1), 558–561.
- (42) Blöchl, P. E. Projector augmented-wave method. *Phys. Rev. B: Condens. Matter Mater. Phys.* **1994**, *50* (24), 17953–17979.
- (43) Perdew, J. P.; Burke, K.; Ernzerhof, M. Generalized gradient approximation made simple. *Phys. Rev. Lett.* **1996**, *77* (18), 3865–3868.
- (44) Kwon, K. C.; Kim, C.; Le, Q. V.; Gim, S.; Jeon, J.-M.; Ham, J. Y.; Lee, J.-L.; Jang, H. W.; Kim, S. Y. Synthesis of atomically thin transition metal disulfides for charge transport layers in optoelectronic devices. *ACS Nano* **2015**, *9*, 4146–4155.
- (45) Kang, S. B.; Kwon, K. C.; Choi, K. S.; Lee, R.; Hong, K.; Suh, J. M.; Im, M. J.; Sanger, A.; Choi, I. Y.; Kim, S. Y.; Shin, J. C.; Jang, H. W.; Choi, K. J. Transfer of ultrathin molybdenum disulfide and transparent nanomesh electrode onto silicon for efficient hetero-junction solar cells. *Nano Energy* **2018**, *50*, 649–658.
- (46) Wang, X.; Lin, J.; Zhu, Y.; Luo, C.; Suenaga, K.; Cai, C.; Xie, L. Chemical vapor deposition of trigonal prismatic NbS₂ monolayers and 3R-polytype few-layers. *Nanoscale* **2017**, *9*, 16607–16611.
- (47) Wu, X.; Tao, Y.; Ke, X.; Zhu, J.; Hong, J. Catalytic synthesis of long NbS₂ nanowire strands. *Mater. Res. Bull.* **2004**, *39* (7–8), 901–908.
- (48) Kim, Y. H.; Park, J. S.; Choi, Y.-R.; Park, S. Y.; Lee, S. Y.; Sohn, W.; Shim, Y.-S.; Lee, J.-H.; Park, C. R.; Choi, Y. S.; et al. Chemically fluorinated graphene oxide for room temperature ammonia detection at ppb levels. *J. Mater. Chem. A* **2017**, *5* (36), 19116–19125.
- (49) Cui, S.; Wen, Z.; Huang, X.; Chang, J.; Chen, J. Stabilizing MoS₂/Nanosheets through SnO₂ Nanocrystal Decoration for High-Performance Gas Sensing in Air. *Small* **2015**, *11* (19), 2305–2313.
- (50) Hu, H.; Trejo, M.; Nicho, M. E.; Saniger, J. M.; Garcia-Valenzuela, A. Adsorption kinetics of optochemical NH₃ gas sensing with semiconductor polyaniline films. *Sens. Actuators, B* **2002**, *82*, 14–23.
- (51) Abbas, A. N.; Liu, B.; Chen, L.; Ma, Y.; Cong, S.; Aroonyadet, N.; Kopf, M.; Nilges, T.; Zhou, C. Black phosphorus gas sensors. *ACS Nano* **2015**, *9*, 5618–5624.
- (52) Li, J.; Lu, Y.; Ye, Q.; Cinke, M.; Han, J.; Meyyappan, M. Carbon nanotube sensors for gas and organic vapor detection. *Nano Lett.* **2003**, *3* (7), 929–933.
- (53) Dua, V.; Surwade, S. P.; Ammu, S.; Agnihotra, S. R.; Jain, S.; Roberts, K. E.; Park, S.; Ruoff, R. S.; Manohar, S. K. All-organic vapor sensor using inkjet-printed reduced graphene oxide. *Angew. Chem., Int. Ed.* **2010**, *49* (12), 2154–2157.
- (54) Cho, S.-Y.; Kim, S. J.; Lee, Y.; Kim, J.-S.; Jung, W.-B.; Yoo, H.-W.; Kim, J.; Jung, H.-T. Highly enhanced gas adsorption properties in vertically aligned MoS₂ layers. *ACS Nano* **2015**, *9*, 9314–9321.
- (55) Long, H.; Harley-Trochimczyk, A.; Pham, T.; Tang, Z.; Shi, T.; Zettl, A.; Carraro, C.; Worsley, M. A.; Maboudian, R. High surface area MoS₂/Graphene hybrid aerogel for ultrasensitive NO₂ detection. *Adv. Funct. Mater.* **2016**, *26*, 5158–5165.
- (56) Schedin, F.; Geim, A. K.; Morozov, S. V.; Hill, E. W.; Blake, P.; Katsnelson, M. I.; Novoselov, K. S. Detection of individual gas molecules adsorbed on graphene. *Nat. Mater.* **2007**, *6*, 652–655.
- (57) Fowler, J. D.; Allen, M. J.; Tung, V. C.; Yang, Y.; Kaner, R. B.; Weiller, B. H. Practical chemical sensors from chemically derived graphene. *ACS Nano* **2009**, *3*, 301–306.
- (58) Akinwande, D.; Petrone, N.; Hone, J. Two-dimensional flexible nanoelectronics. *Nat. Commun.* **2014**, *5*, 5678.
- (59) Lemmon, E. W.; McLinden, M. O.; Friend, D. G.; Linstrom, P.; Mallard, W. *NIST Chemistry Web Book, Nist standard reference database number 69*; National Institute of Standards and Technology; Gaithersburg, MD, 2011, <http://www.webbook.nist.gov/chemistry/>.